Band shifting for ocean color multi-spectral reflectance data

Frédéric Mélin,[1] **and Gert Sclep**[1,2]

[1]*European Commission, Joint Research Centre (JRC), Institute for Environment and Sustainability (IES), TP270, via Fermi 2749, Ispra 21027, Italy*
[2]*now at: European Commission, Publications Office of the European Union, 2 rue Mercier, Luxemburg, L-2985, Luxembourg*
*frederic.melin@jrc.ec.europa.eu

Abstract: An approach to perform band shifting applied to multi-spectral ocean remote sensing reflectance R_{RS} values in the visible spectral range is presented. The band-shifting scheme aims at expressing R_{RS} at a wavelength not originally part of the spectrum from data at neighboring bands. The scheme relies on the determination of inherent optical properties (IOPs) by a bio-optical model, the calculation of the IOPs at the target wavelength using the spectral shapes assumed for each IOP, and the operation of the bio-optical model in forward mode to express R_{RS} at the target wavelength. The performance of the band-shifting scheme applied to bands typical of satellite missions is assessed with hyper-spectral data sets obtained from radiative transfer simulations or from field measurements. The relative error ε on the conversion factors from 488 to 490 nm is mostly within 1%. Analogous results are obtained for conversions in the red spectral domain (665, 667 and 670 nm) only for synthetic data sets. The range of ε for conversions between green bands (547, 555 and 560 nm) is within 2% to 5% depending on the data set considered. Similar results are obtained when R_{RS} values are computed at 510 nm from data at 488 and 531 nm. In the case of the assessment with simulated data, all band-shifting operations are characterized by an ε range within 2% for all conversions when the concentration of chlorophyll-*a* is lower than 1 mg m^{-3}. Applied to satellite data, the band-shifting scheme noticeably improves the agreement between R_{RS} data from different missions.

OCIS codes: (010.0010) Atmospheric and oceanic optics; (280.4788) Optical sensing and sensors.

References and links

1. GCOS, "Systematic observation requirements for satellite-based data products for climate, 2011 update: Supplemental details to the satellite-based component of the Implementation Plan for the Global Observing System for Climate in Support of the UNFCCC", Tech. Rep. **154**, World Meteorological Organization (2011).
2. W. E. Esaias, M. R. Abbott, I. Barton, O. B. Brown, J. W. Campbell, K. L. Carder, D. K. Clark, R. H. Evans, F. E. Hoge, H. R. Gordon, W. M. Balch, R. Letelier, and P. J. Minnett, "An overview of MODIS capabilities for ocean science observations," IEEE Trans. Geosci. Remote Sens. **36,** 1250–1265 (1998).
3. C. R. McClain, M. L. Cleave, G. C. Feldman, W. W. Gregg, S. B. Hooker, and N. Kuring, "Science quality SeaWiFS data for global biosphere research," Sea Tech. **39,** 10–16 (1998).
4. M. Rast, J. L. Bezy, and S. Bruzzi, "The ESA Medium Resolution Imaging Spectrometer MERIS - A review of the instrument and its mission," Int. J. Remote Sens. **20,** 1681–1702 (1999).

#223013 - $15.00 USD Received 11 Sep 2014; revised 7 Nov 2014; accepted 7 Nov 2014; published 28 Jan 2015

5. F. Mélin, V. Vantrepotte, M. Clerici, D. D'Alimonte, G. Zibordi, J.-F. Berthon and E. Canuti, "Multi-sensor satellite time series of optical properties and chlorophyll *a* concentration in the Adriatic Sea," Prog. Oceanogr. **91**, 229-244 (2011).
6. G. Zibordi, J.-F. Berthon, F. Mélin, D. D'Alimonte, and S. Kaitala, "Validation of satellite ocean color primary products at optically complex coastal sites: northern Adriatic Sea, northern Baltic Proper, Gulf of Finland," Remote Sens. Environ. **113**, 2574–2591 (2009).
7. G. Zibordi, J.-F. Berthon, F. Mélin, and D. D'Alimonte, "Cross-site consistent in situ measurements for satellite ocean color applications: The BiOMaP radiometric dataset," Remote Sens. Environ. **115,** 2104–2115 (2011).
8. F. Mélin, G. Zibordi, J.-F. Berthon, S.W. Bailey, B.A. Franz, K.J. Voss, S. Flora, and M. Grant, "Assessment of MERIS reflectance data as processed by SeaDAS over the European Seas," Opt. Exp. **19**, 25657-25671 (2011).
9. D. Antoine, F. d'Ortenzio, S. B. Hooker, G. Bécu, B. Gentili, D. Tailliez, and A. J. Scott, "Assessment of uncertainty in the ocean reflectance determined by three satellite ocean color sensors (MERIS, SeaWiFS and MODIS-A) at an offshore site in the Mediterranean Sea (BOUSSOLE project)," J. Geophys. Res. **113**, C07013, 10.1029/2007JC004472 (2008).
10. A. Morel and S. Maritorena, "Bio-optical properties of oceanic waters: A reappraisal," J. Geophys. Res. **106**, 7163-7180 (2001).
11. A. Morel, Y. Huot, B. Gentili, P.J. Werdell, S.B. Hooker and B.A. Franz, "Examining the consistency of products derived from various ocean color sensors in open ocean (Case 1) waters in the perspective of a multi-sensor approach," Remote Sens. Env. **111** 69-88 (2007).
12. Z.-P. Lee, K.L. Carder, and R.A. Arnone, "Deriving inherent optical properties from water color: A multiband quasi-analytical algorithm for optically deep waters," Appl. Opt. **41**, 5755-5772 (2002).
13. H.R. Gordon, O.B. Brown, R.H. Evans, J.W. Brown, R.C. Smith, K.S. Baker, and D.S. Clark, "A semi-analytic radiance model of ocean color," J. Geophys. Res. **93**, 10909-10924 (1988).
14. X. Zhang, L. Hu, and M.-X. He, "Scattering by pure seawater: Effect of salinity," Opt. Exp. **17**, 5698-5710 (2009).
15. R.M. Pope and E.S. Fry, "Absorption spectrum (380-700 nm) of pure water. II. Integrating cavity measurements. Appl. Opt., **36**, 8710-8723 (1997).
16. Z.-P. Lee, B. Lubac, P.J. Werdell, and R.A. Arnone, "An update of the Quasi-Analytical Algorithm (QAA_v5)," Tech. Rep. International Ocean-Colour Coordinating Group, 2009 (http://www.ioccg.org/groups/software.html).
17. Z.-P. Lee, R. Arnone, C. Hu, P.J. Werdell, and B. Lubac, "Uncertainties of optical parameters and their propagations in an analytical ocean color inversion algorithm," Appl. Opt. **49**, 369-381 (2010).
18. A. Bricaud, M. Babin, A. Morel, H. Claustre, "Variability in the chlorophyll-specific absorption coefficients of natural phytoplankton: Analysis and parameterization," J. Geophys. Res. **100**, 13321-13332 (1995).
19. F. Mélin, G. Zibordi, and J.-F. Berthon, "Assessment of satellite ocean color products at a coastal site," Remote Sens. Environ. **110**, 192-215 (2007).
20. R.W. Brewin, S. Sathyendranath, D. Mueller, C. Brockmann, P.-Y. Deschamps, E. Devred, R. Doerffer, N. Fomferra, B. Franz, M. Grant, S. Groom, A. Horseman, C. Hu, H. Krasemann, Z.-P. Lee, S. Maritorena, F. Mlin, M. Peters, T. Platt, P. Regner, T. Smyth, F. Steinmetz, J. Swinton, P.J. Werdell, G.N. White, "The Ocean Colour Climate Change Initiative. III. A round-robin comparison on in-water bio-optical algorithms," Remote Sens. Environ., 10.1016/j.rse.2013.09.016, in press (2014).
21. C.D. Mobley, "Light and water," Academic Press, 592p. (1994).
22. IOCCG, "Remote sensing of inherent optical properties: Fundamentals, tests of algorithms, and applications," Reports of the International Ocean Colour Coordinating Group, Number **5**, Lee, Z.-P. (Ed.) 126 pp., IOCCG, Dartmouth, Canada (2006).
23. P.J. Werdell, S.W. Bailey, G.S. Fargion, C. Pietras, K.D. Knobelspiesse, G.C. Feldman, and C.R. McClain, "Unique data repository facilitates ocean color satellite validation," EOS Trans. of the Am. Geophys. Union **84**, 377 (2003).
24. D. K. Clark, H. R. Gordon, K. J. Voss, Y. Ge, W. Broenkow, and C. Trees, "Validation of atmospheric correction over the oceans," J. Geophys. Res. **102**, D14, 17209–17217 (1997).
25. S. W. Brown, S. J. Flora, M. J. Feinholz, M. A. Yarbrough, T. Houlihan, D. Peters, Y. S. Kim, J. L. Mueller, C. B. Johnson, and D. K. Clark, "The Marine Optical BuoY (MOBY) radiometric calibration and uncertainty budget for ocean color satellite sensor vicarious calibration," in *Sensors, Systems, and Next-Generation Satellites XI*, R. Meynart, S. P. Neeck, H. Shimoda, and S. Habib, eds., Proc. SPIE **6744**, pp. 67441M (2007).
26. G. Thuillier, M. Hersé, P.C. Simon, D. Labs, H. Mandel, D. Gillotay, and T. Foujols, "The solar spectral irradiance from 200 to 2400 nm as measured by the SOLSPEC spectrometer from the ATLAS 1-2-3 and EURECA missions," Solar Physics **214**, 1-22 (2003).
27. M. Wang, B.A. Franz, R.A. Barnes, "Analysis of the SeaWiFS spectral band-pass effects," NASA Tech. Mem. 2000-206892, vol. 10, chap. 2, 6-11, Goddard Space Flight Center, Greenbelt, MD (2000).
28. A. Morel, D. Antoine, and B. Gentili, "Bidirectional reflectance of oceanic waters: accounting for Raman emission and varying particle scattering phase function," Appl. Opt. **41**, 6289–6306 (2002).
29. M. Wang, B.A. Franz, R.A. Barnes, and C.R. McClain, "Effects of spectral bandpass on SeaWiFS-retrieved near-surface optical properties of the ocean," Appl. Opt. **40** 343–348 (2001).

#223013 - $15.00 USD Received 11 Sep 2014; revised 7 Nov 2014; accepted 7 Nov 2014; published 28 Jan 2015

30. B.A. Franz, R.E. Eplee, S.W. Bailey, and M. Wang, "Changes to the atmospheric correction algorithm and retrieval of oceanic optical properties," NASA Tech. Mem. 2003-206892, vol. 22, chap. 5, 29-33, Goddard Space Flight Center, Greenbelt, MD (2003).
31. S.B. Hooker and C.R. McClain, "The calibration and validation of SeaWiFS data," Prog. Oceanogr. **45**, 427-465 (2000).
32. R. Hollmann, C.J. Merchant, R. Saunders, C. Downy, M. Buchwitz, A. Cazenave, E. Chuvieco, P. Defourny, G. de Leeuw, R. Forsberg, T. Holzer-Popp, F. Paul, S. Sandven, S. Sathyendranath, M. van Roozendael, and W. Wagner, "The ESA Climate Change Initiative - Satellite data records for essential climate variables," Bull. Am. Meteo. Soc. **94**, 1541-1552 (2013).
33. S. Maritorena, D.A. Siegel, and A.R. Peterson, "Optimization of a semi-analytical ocean color model for global-scale applications," Appl. Opt. **41**, 2705–2714 (2002).
34. P.J. Werdell, B.A. Franz, S.W. Bailey, G.C. Feldman, E. Boss, V.E. Brando, M.D. Dowell, T. Hirata, S.J. Lavender, Z.-P. Lee, H. Loisel, S. Maritorena, F. Mélin, T.S. Moore, T.J. Smyth, D. Antoine, E. Devred, O. Fanton d'Andon, and A. Mangin, "Generalized ocean color inversion model for retrieving marine inherent optical properties," Appl. Opt. **52**, 2019–2037 (2013).
35. F. Mélin and G. Zibordi, "An optically-based technique for producing merged spectra of water leaving radiances from ocean color," Appl. Opt. **46**, 3856–3869 (2007).
36. F. Mélin, G. Zibordi, and S. Djavidnia, "Merged series of normalized water leaving radiances obtained from multiple satellite missions for the Mediterranean Sea," Adv. Space Res. **43,** 423–437 (2009).
37. Z.-P. Lee, S. Shang, C. Hu, and G. Zibordi, "Spectral interdependence of remote-sensing reflectance and its implications on the design of ocean color satellite sensors," App. Opt. **53** 3301-3310 (2014).
38. F. Mélin and B.A. Franz, "Assessment of satellite ocean colour radiometry and derived geophysical products," in *Optical Radiometry for Oceans Climate Measurements*, chap. 6.1, G. Zibordi, C. Donlon, and A. Parr, eds., Academic Press, Experimental Methods in the Physical Sciences vol. 47, 722 pp. (2014).
39. W. Chen and R. Lucke, "Out-of-band correction for multispectral remote sensing," IEEE Trans. Geosci. Remote Sens. **51** 2476-2483 (2013).
40. W. Chen and B.-C. Gao, "A multispectral decomposition technique for the recovery of true SeaWiFS top-of-atmosphere radiances," IEEE Geosci. Remote Sens. Lett. **10** 288-292 (2013).

1. Introduction

Water-leaving radiance, or equivalently remote sensing reflectance, is among the Essential Climate Variables (ECV) [1]. Considering that a satellite mission lifetime is typically five to ten years, the creation of long-term time series has to rely on a suite of subsequent missions with a sufficient period of overlap to allow the determination of inter-mission differences. The various ocean color missions that have been in operation have a different set of bands, which is an obstacle to a quantitative comparison of their respective records of remote sensing reflectance R_{RS}. While some center wavelengths coincide, others differ by more than 10 nm if the recent global ocean color missions are considered, the Moderate Resolution Spectroradiometer (MODIS [2]), the Sea-viewing Wide Field-of-View Sensor (SeaWiFS, [3]) and the Medium Resolution Imaging Spectrometer (MERIS, [4]). For instance the green ocean color band, which is often used as a reference band for bio-optical algorithms, is centered respectively at 547, 555 and 560 nm for these three missions. In practice it is not straightforward to know for example if the MODIS R_{RS} value at 547 nm is actually too low or high with respect to a coincident SeaWiFS R_{RS} at 555 nm.

Accounting for band differences is thus essential to assessing the multi-mission ocean color data record. Correcting for band differences, a process referred to as band shifting, can also be a pre-processing step before merging R_{RS} spectra from different missions [5]. Band shifting is important in validation activities where the bands associated with field observations do not necessarily coincide with those of the satellite sensors. Consequently, band-shifting schemes have been developed for validation analyzes. Some of these approaches rely on a reflectance model and bio-optical relationships proposed for a specific region [6, 7, 8] or for relatively clear open ocean waters [9]. In the context of a Case-1 water model [10], all optical properties are well defined and a certain spectral shape for R_{RS} is expected for each value of the chlorophyll-a concentration (Chl*a*). This allows the definition of a set of consistent algorithms for the different

#223013 - $15.00 USD Received 11 Sep 2014; revised 7 Nov 2014; accepted 7 Nov 2014; published 28 Jan 2015

sensors and their respective bands [11]. However it is desirable to have a framework for band shifting that is more generally applicable. The performance of a band-shifting scheme also needs to be assessed so that its contribution to the uncertainty budgets can be quantified.

The objective of this work is to present an approach to perform band shifting applied to multi-spectral R_{RS} values in the visible spectral range. The method that relies on a bio-optical algorithm, the Quasi-Analytical Algorithm (QAA), is first introduced. Then its performance is analyzed using synthetic data as well as field observations. Finally, its application to satellite data is illustrated.

2. Methods

2.1. Description of the Band-Shifting Scheme

The principle of the scheme is to take advantage of spectral shapes known for inherent optical properties (IOPs) to perform the band-shifting process. A bio-optical algorithm allows the inversion of the apparent optical property (AOP) R_{RS} expressed at wavelengths λ to derive IOPs at the same set of wavelengths, including a reference wavelength λ_r; IOPs at the desired (target) wavelength λ_t, close to one of the λ's (called the input wavelength λ_i), are then computed, and the bio-optical algorithm can be applied in its forward mode to produce R^f_{RS}, finally leading to an estimate of R_{RS} at the target wavelength (R^e_{RS}).

First the remote sensing reflectance R_{RS}, a quantity expressed above the sea surface, is related to the below-water reflectance r_{rs} (ratio of below-water upwelling radiance and downward irradiance):

$$r_{rs}(\lambda) = \frac{R_{RS}(\lambda)}{T + rQ(\lambda)R_{RS}(\lambda)} \tag{1}$$

where T accounts for the radiance transmittance through the air-water interface, r is the water-to-air Fresnel reflection coefficient, and Q is the ratio of below-water upwelling radiance and irradiance. For the sake of simplicity, geometry (zenith and azimuth angles) is omitted from this equation. As in [12], approximations are made with $T \approx 0.52$ and $rQ \approx 1.7$.

Following [13], the relationship between AOPs and IOPs is expressed as:

$$r_{rs}(\lambda) = g_0 \frac{b_b(\lambda)}{b_b(\lambda) + a(\lambda)} + g_1 [\frac{b_b(\lambda)}{b_b(\lambda) + a(\lambda)}]^2 \tag{2}$$

where a and b_b are the total absorption and backscattering coefficients, respectively. These coefficients are partitioned into separate contributions, b_b being the sum of the backscattering due to pure seawater b_{bw} and to particles b_{bp}, and a being the sum of absorption due to pure seawater a_w, phytoplankton a_{ph} and colored detrital matter (CDM) a_{cdm} (itself due to chromophoric dissolved organic matter, CDOM, and non-pigmented particles). The IOPs b_{bw} and a_w for seawater are spectral constants, obtained from [14] and [15], respectively. The coefficients g_0 and g_1 are taken equal to 0.08945 and 0.1247, respectively [12]. Inverting Eq. (2) to obtain the various IOP components at any wavelength λ associated with R_{RS} is performed by the Quasi-Analytical Algorithm (QAA) (version 5, [12, 16, 17]).

The QAA relies on assumptions describing the spectral shapes of b_{bp} and a_{cdm} but does not assume any shape for a_{ph}. The band shifting thus needs an additional assumption characterizing the spectral shape of a_{ph}, taken from [18]. Therefore IOPs at 2 different wavelengths λ (where IOPs are known) and λ_t can be related as follows:

$$b_{bp}(\lambda_t) = b_{bp}(\lambda)(\frac{\lambda}{\lambda_t})^{\eta} \tag{3}$$

$$a_{ph}(\lambda_t) = A(\lambda_t)(\frac{a_{ph}(\lambda)}{A(\lambda)})^{\frac{1-B(\lambda_t)}{1-B(\lambda)}} \tag{4}$$

#223013 - $15.00 USD Received 11 Sep 2014; revised 7 Nov 2014; accepted 7 Nov 2014; published 28 Jan 2015

$$a_{cdm}(\lambda_t) \quad = \quad a_{cdm}(\lambda)e^{-S(\lambda_t-\lambda)} \tag{5}$$

The spectral shape of b_{bp} and a_{cdm} are defined by η and S, respectively, that are defined by empirical relationships from r_{rs} [16]. In Eq. (4), A and B are constant tabulated spectral values from [18]. All terms on the right-hand side of Eqs. (3)-(5) are thus known.

Given a spectrum R_{RS} provided at several wavelengths including λ_i and a reference wavelength λ_r (selected as 443 nm), R_{RS} at the target wavelength λ_t close to λ_i is computed as follows:

1. the QAA is applied to solve Eq. (2) providing b_{bp}, a_{ph} and a_{cdm} at λ_r;
2. b_{bp}, a_{ph} and a_{cdm} are calculated at λ_i and λ_t using Eqs. (3)-(5) where λ is substituted by λ_r;
3. Eqs. (2) and (1) are applied to obtain forward-mode values of R_{RS}, R^f_{RS}, at λ_i and λ_t;
4. the estimated value of R_{RS} at λ_t is finally expressed as:

$$R^e_{RS}(\lambda_i \rightarrow \lambda_t) = R^f_{RS}(\lambda_t)\frac{R_{RS}(\lambda_i)}{R^f_{RS}(\lambda_i)} \tag{6}$$

where the $\rightarrow$ sign indicates the operation of band shifting to convert R_{RS} from one band to another. The correction in item 4 (Eq. (6)) is necessary to ensure that the estimated R^e_{RS} is equal to R_{RS} for λ_t=λ_i. After item 3, this is not ensured since the a_{ph} value estimated at λ_i from the value at λ_r=443 nm by Eq. (4) is not necessarily the a_{ph} output of QAA. An alternative would be to choose λ_r as λ_i for each band-shifting action (thus item 4 would not be necessary). But the performance of the QAA in terms of a_{ph} retrieval is degraded for longer wavelengths (particularly in the red domain) [19, 20], so that it appears more suitable to select λ_r equal to 443 nm, a wavelength where the QAA performs reasonably well.

The application of the band shifting is intended for bridging fairly small spectral differences. The case of the MODIS band at 531 nm is peculiar, having no equivalent in other sensors: the nearest wavelengths for SeaWiFS or MERIS are distant $\sim$20 nm. Conversely, there is a difference of $\sim$20 nm between the 510-nm band of SeaWiFS or MERIS and the nearest MODIS bands. In these cases, the band shifting is operated twice, from the wavelengths lower and higher than the target wavelength. The estimated R_{RS} is then a weighted average of the two values. Specifically, the estimated value of SeaWiFS and MERIS R_{RS} at λ_t=531 nm is written as:

$$R^e_{RS}(531) = \frac{(\lambda_2 - 531)R^e_{RS}(\lambda_1 \rightarrow 531) + (531 - \lambda_1)R^e_{RS}(\lambda_2 \rightarrow 531)}{\lambda_2 - \lambda_1} \tag{7}$$

The value of λ_1 is 510 nm for SeaWiFS and MERIS, while λ_2 is 555 nm and 560 nm, respectively.

Similarly, a MODIS R_{RS} at 510 nm is obtained as:

$$R^e_{RS}(510) = \frac{(531 - 510)R^e_{RS}(488 \rightarrow 510) + (510 - 488)R^e_{RS}(531 \rightarrow 510)}{531 - 488} \tag{8}$$

the band shifting being operated from 488 and 531 nm to 510 nm.

#223013 - $15.00 USD Received 11 Sep 2014; revised 7 Nov 2014; accepted 7 Nov 2014; published 28 Jan 2015

2.2. Assessment Method

This study attempts to characterize the performance of the band-shifting scheme. This can be tested assuming that a data set with the required spectral resolution is available. The assessment is performed by comparing the estimated R^e_{RS} and the true R_{RS} at the target wavelength λ_t, the relative difference between the two terms being (in %):

$$\varepsilon(\lambda_i \rightarrow \lambda_t) = 100.\frac{R^e_{RS}(\lambda_t) - R_{RS}(\lambda_t)}{R_{RS}(\lambda_t)} \tag{9}$$

If $R^e_{RS}(\lambda_t)$ is substituted by $R_{RS}(\lambda_i)$, the reflectance value at the input wavelength λ_i, Eq. (9) expresses the relative difference between R_{RS} at the two wavelengths λ_i and λ_t,

$$\varepsilon(\lambda_i, \lambda_t) = 100.\frac{R_{RS}(\lambda_i) - R_{RS}(\lambda_t)}{R_{RS}(\lambda_t)} \tag{10}$$

The relative difference in Eq. (9) can be interpreted equivalently in terms of the conversion factor C_f that quantifies the band shifting:

$$\varepsilon(\lambda_i \rightarrow \lambda_t) = 100.\frac{C^e_f(\lambda_i \rightarrow \lambda_t) - C_f(\lambda_i, \lambda_t)}{C_f(\lambda_i, \lambda_t)} \tag{11}$$

where the true conversion factor between the input wavelength λ_i and the target wavelength λ_t, $C_f(\lambda_i, \lambda_t)$, is $R_{RS}(\lambda_t)/R_{RS}(\lambda_i)$, and the conversion factor estimated by band shifting, $C^e_f(\lambda_i \rightarrow \lambda_t)$, is $R^e_{RS}(\lambda_i \rightarrow \lambda_t)/R_{RS}(\lambda_i)$. Substituting $C^e_f(\lambda_i \rightarrow \lambda_t)$ by C_f=1 in Eq. (11) is equivalent to Eq. (10) and expresses the error done by assuming equality between $R_{RS}(\lambda_i)$ and $R_{RS}(\lambda_t)$, i.e., if no conversion is performed.

If $R^e_{RS}(\lambda_t)$ is computed from R_{RS} at two bands λ_1 and λ_2 because of large spectral differences, ε is written as a linear combination of conversion factors in line with Eqs. (7) or (8):

$$\varepsilon(\lambda_1, \lambda_2 \rightarrow \lambda_t) = 100.[\frac{\lambda_2 - \lambda_t}{\lambda_2 - \lambda_1}\frac{C^e_f(\lambda_1 \rightarrow \lambda_t) - C_f(\lambda_1, \lambda_t)}{C_f(\lambda_1, \lambda_t)} + \frac{\lambda_t - \lambda_1}{\lambda_2 - \lambda_1}\frac{C^e_f(\lambda_2 \rightarrow \lambda_t) - C_f(\lambda_2, \lambda_t)}{C_f(\lambda_2, \lambda_t)}] \tag{12}$$

Eq. (12) is also equivalent to Eq. (9).

For all spectral conversions, the ε distributions will be compared with respect to a reference case where no conversion is performed, considering that $R_{RS}(\lambda_i)$ can be used instead of $R_{RS}(\lambda_t)$ (meaning C_f=1, or Eq. (10)). When two bands are used because of a large spectral difference, the performance of the band-shifting scheme (Eqs. (7) or (8)) is evaluated with respect to operating a simple linear interpolation by which R_{RS} at λ_t is written as:

$$R^{int}_{RS}(\lambda_t) = \frac{(\lambda_2 - \lambda_t)R_{RS}(\lambda_1) + (\lambda_t - \lambda_1)R_{RS}(\lambda_2)}{\lambda_2 - \lambda_1} \tag{13}$$

For that reference case, ε is simply computed by substituting $R_{RS}(\lambda_i)$ by $R^{int}_{RS}(\lambda_t)$ in Eq. (10).

3. Data

The assessment of a band-shifting scheme relies on the availability of data sets with the required spectral resolution. One way of circumventing this difficulty is to create synthetic hyper-spectral data, a step which is first described. Then, suitable field observations are introduced.

#223013 - $15.00 USD Received 11 Sep 2014; revised 7 Nov 2014; accepted 7 Nov 2014; published 28 Jan 2015

3.1. Synthetic Data Sets

Two sets of synthetic data were developed using radiative transfer (RT) simulations performed with the RT HydroLight code [21]. The first one reproduces Case-1 conditions, where all optical properties are defined by the value of Chl*a* [10], varied between 0.03 and 30 mg m^{-3} (20 values, by steps of approximately 0.15 units of logarithm in base 10). A broader range of optical properties is represented by the data set developed in the framework of an International Ocean-Colour Coordinating Group (IOCCG) exercise of bio-optical algorithm testing [22]. This data set contains 500 different optical conditions associated with the same 20 levels of Chl*a* values. Differently from the Case-1 conditions, scattering by inorganic particles and absorption by CDOM and detritus were allowed to vary independently from Chl*a* within certain typical ranges of variability. Together these synthetic data should cover a large part of the optical variability found in the ocean (see [22]). For illustration, Fig. 1(a) shows the average R_{RS} spectrum for each level of Chl*a*.

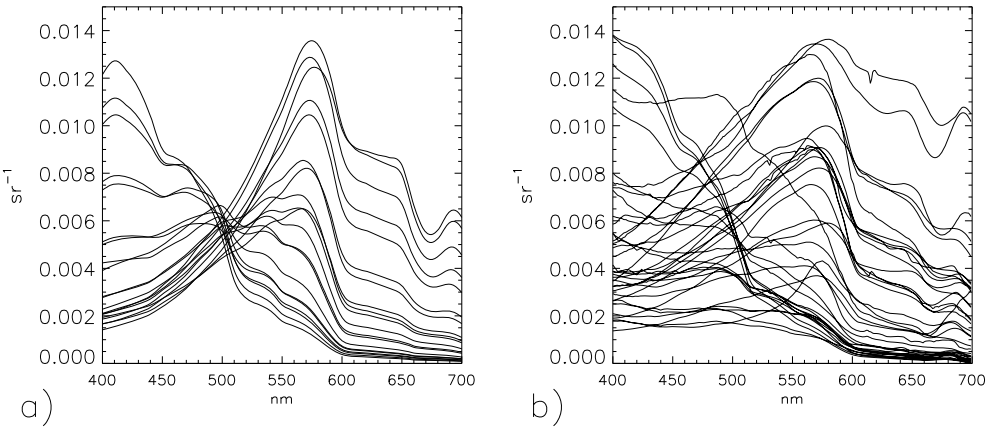

Fig. 1. a) Average R_{RS} spectrum associated with each Chl*a* value of the IOCCG synthetic data; b) Average R_{RS} spectrum of each measurement campaign selected for analysis within SeaBASS.

All IOPs were first expressed at a 1-nm resolution; the RT simulations were then conducted at this resolution with each set of IOPs to produce a hyper-spectral set of R_{RS}. For phytoplankton scattering a Fournier-Forand phase function with backscattering ratio of 0.01 was selected; for mineral scattering the average Petzold particle phase function was used. Wind speed was set to 5 m s^{-1} and the Sun zenith angle to 30°. All other parameters kept their HydroLight default values.

For completeness, it is recalled that the synthetic data set created for the IOCCG exercise [22] has been used in QAA version 5 to define a relationship calculating the total absorption at the green band from R_{RS}, which is the first step in the QAA inversion procedure. However, other parameters of the algorithms, like those defining the spectral shapes, are independent of this data set. It is as well noted that the performance of the QAA has not changed largely through its different versions [12, 16, 19, 20, 22], so that the results presented for this synthetic data set should be valid.

#223013 - $15.00 USD Received 11 Sep 2014; revised 7 Nov 2014; accepted 7 Nov 2014; published 28 Jan 2015

3.2. Field Data

The SeaWiFS Bio-optical Archive and Storage System (SeaBASS, [23]) of the National Aeronautics and Space Administration (NASA) was searched for hyperspectral data that could be suitable to test the band-shifting scheme. The selected data were above-water radiometric measurements gathered through US programs associated with the Bermuda Bio-Optics Program (BBOP), the National Oceanic and Atmospheric Administration (NOAA), the Naval Research Laboratory (NRL), and the University of South Florida (USF). R_{RS} data were selected if they provided spectral values between 400 and 700 nm with a spectral resolution nowhere exceeding 5 nm. Some spectra were also excluded after visual inspections. The selected R_{RS} data, totalling 783 spectra from 36 measurement campaigns between 1998 and 2010, were then expressed on a common 1-nm grid before being converted as sensor-specific spectra assuming a bandwidth of $\pm$5-nm. Fig. 1(b) illustrates the optical variability represented by this data set by showing an average spectrum for each campaign, covering waters from coastal North America, Venezuela, northern Adriatic and southern Atlantic Ocean. Some spectra show a maximum in the blue spectral domain as associated with clear ocean waters, while some spectra are associated with coastal regions and display maxima beyond 550 nm and fairly high R_{RS} value in the red part of the spectral range.

Additionally, data collected by the Marine Optical BuoY (MOBY) [24] were considered. The buoy is operating in deep oligotrophic waters offshore Lanai (Hawaii) providing regular and accurate measurements for this type of conditions [25]. Radiance values are derived from underwater hyper-spectral radiometric measurements (340-955 nm) at fixed depths along with above-water solar incident irradiance. They are then convolved with the spectral response of various space sensors to provide SeaWiFS, MODIS or MERIS-like normalized water-leaving radiance L_{WN}. These sensor-specific data are suitable to test the band-shifting scheme. For example, the R_{RS} values associated with MODIS (onboard Aqua) for one measurement station can be expressed on the wavelengths of MERIS by band shifting, and then compared with R_{RS} provided by the MOBY project for MERIS at that measurement station.This is not as ideal as working with truly hyper-spectral data, but it mimics well the type of conversions that might be attempted between remotely-sensed R_{RS} associated with different satellite missions. The analysis relied on the so-called "in-band" data (limiting the relative spectral response to within 1% of its maximum), and kept only data flagged as "good". The conversion from L_{WN} to R_{RS} was performed with the extra-terrestrial solar irradiance values from [26]. The analyzed data are those associated with the MODIS-Aqua and MERIS bands (2934 records), as SeaWiFS has a more significant out-of-band response [27].

For all field measurements, bidirectional effects (dependence on illumination condition and seawater optical anisotropy) were not corrected. This would require functions relating R_{RS} observed with different observation and illumination geometries, such as those proposed in [28] that are indexed as a function of Chl*a*. Besides the requirement for a hyper-spectral resolution, the application of such functions would result in approximations that could affect the spectral shape of R_{RS} and consequently the results of the current work. Since all comparisons are made with consistent geometries, the absence of correction does not entail any limitations of the analysis. Finally, it is noted that the considered field measurements have not been used for the definition of the QAA.

3.3. Satellite Data

For illustration, the band-shifting scheme was applied to satellite data. SeaWiFS and MODIS-Aqua daily R_{RS} binned Level-3 data were obtained from the Ocean Biology Processing Group (OBPG) of NASA for the year 2003 (processing R2010 and R2012, respectively). All coincident SeaWiFS/MODIS data pairs were accumulated on a grid of 12^{th}-degree resolution,

#223013 - $15.00 USD Received 11 Sep 2014; revised 7 Nov 2014; accepted 7 Nov 2014; published 28 Jan 2015

amounting to 49.8 million of R_{RS} matching pairs. In the operational processing, differences in spectral response are accounted for by an out-of-band correction expressing R_{RS} values onto a 10-nm square band-pass [29, 30]. The band-shifting scheme was operated on all MODIS spectra to produce synthetic MODIS data that could be directly compared with the concurrent SeaWiFS spectra.

4. Results

4.1. Assessment with Synthetic Data Sets

The band-shifting scheme was assessed by analyzing the distribution of the relative difference between estimated and true conversion factors, ε. For comparison, ε was also computed for the case without conversion, i.e., assuming that R_{RS} at the input wavelength can be used as an approximation for R_{RS} at the target wavelength, or by simple linear interpolation when two wavelengths are used (Eq. (13)). Associated with the RT simulations for the Case-1 and IOCCG conditions, respectively, Tables 1 and 2 list ε (median and percentiles) for a full set of conversions that could be used to reconcile R_{RS} from SeaWiFS, MODIS or MERIS. Fig. 2 shows box-and-whiskers plots summarizing for selected conversions the statistical distribution of ε with minimum and maximum, standard deviation, median and 10^{th} and 90^{th} percentiles.

Table 1. Statistics for the Case-1 data set. The three columns are for all conditions, Chl*a*≤1 mg m^{-3} and Chl*a*>1 mg m^{-3}. For each conversion, the first line provides ε (median [10^{th};90^{th} percentiles]) for the reference case (no conversion or linear interpolation), while the second line provides the results obtained by operating the band-shifting scheme. Each conversion is indicated by the input wavelength(s) → target wavelength, together with the typical sensors for which such a conversion would be applied, with A, M and S standing for MODIS, MERIS and SeaWiFS, respectively.

$\lambda \rightarrow \lambda_t$	ε [%]	ε [%]; Chla≤1	ε [%]; Chla>1
488 → 490	-0.7 [-1.7;+2.6]	+1.4 [-0.0;+3.0]	-1.5 [-1.7;-0.9]
(A → S/M)	-0.5 [-1.0;+0.0]	-0.0 [-0.4;+0.0]	-0.8 [-1.1;-0.6]
488/531 → 510	+5.1 [+2.3;+26.8]	+14.7 [+4.7;+30.8]	+3.8 [+2.0;+5.6]
(A → S/M)	+2.2 [+1.4;+5.0]	+1.8 [+1.2;+2.1]	+3.4 [+1.7;+5.6]
510/555 → 531	-0.9 [-4.2;+6.1]	+2.1 [-2.6;+7.1]	-2.1 [-4.3;+0.7]
(S → A)	-0.5 [-3.0;+0.8]	+0.5 [+0.2;+0.9]	-2.4 [-3.1;-0.7]
547 → 555	+5.1 [-5.7;+15.2]	+12.7 [+8.4;+15.8]	-1.7 [-6.4;+3.8]
(A → S)	-1.0 [-1.7;-0.4]	-1.3 [-1.6;-1.0]	-0.5 [-1.9;-0.4]
547 → 560	+7.1 [-7.6;22.2]	+18.3 [+11.8;+23.1]	-2.3 [-8.5;+5.3]
(A → M)	-0.3 [-2.0;+1.1]	-1.6 [-2.2;-0.9]	+0.7 [-0.1;+1.2]
560 → 555	-1.8 [-5.7;+2.0]	-4.7 [-6.0;-3.1]	+1.1 [-1.4;+2.3]
(M → S)	-0.4 [-2.0;+0.5]	+0.4 [+0.1;+0.6]	-1.5 [-2.0;-0.6]
665 → 670	+4.3 [+3.5;+5.6]	+4.0 [+3.5;+4.6]	+4.6 [+3.5;+5.9]
(M → S)	-1.4 [-2.0;-0.5]	-0.8 [-1.3;-0.4]	-1.7 [-2.1;-1.4]
667 → 670	+2.5 [+2.1;+3.3]	+2.4 [+2.1;+2.6]	+2.8 [+2.1;+3.5]
(A → S)	-0.7 [-0.9;-0.3]	-0.5 [-0.7;-0.3]	-0.8 [-0.9;-0.7]
667 → 665	-1.7 [-2.2;-1.4]	-1.5 [-1.8;-1.4]	-1.7 [-2.3;-1.4]
(A → M)	+0.6 [+0.2;+1.3]	+0.3 [+0.1;+0.6]	+1.0 [+0.7;+1.4]

For the conversion 488→490, typically associated with MODIS and SeaWiFS or MERIS, band shifting provides improved estimates of R_{RS} with respect to the reference case where no

#223013 - $15.00 USD Received 11 Sep 2014; revised 7 Nov 2014; accepted 7 Nov 2014; published 28 Jan 2015

conversion is applied (C_f=1) (Fig. 2(a)). The median ε is decreased in modulus to approximately -0.5% for both sets (Case-1 and IOCCG), and is only slightly higher for Chl$a$>1 mg m^{-3} (approximately -1%). The range of ε values is reduced too, the distance between 10^{th} and 90^{th} percentiles (inter-percentile range) being 1% to 1.5% whereas it exceeds 4% if no conversion is applied. Band shifting results in an amplitude of ε ($|\varepsilon|$) lower in 79% of the cases for the Case-1 water conditions, and in 93% of the cases for the IOCCG set.

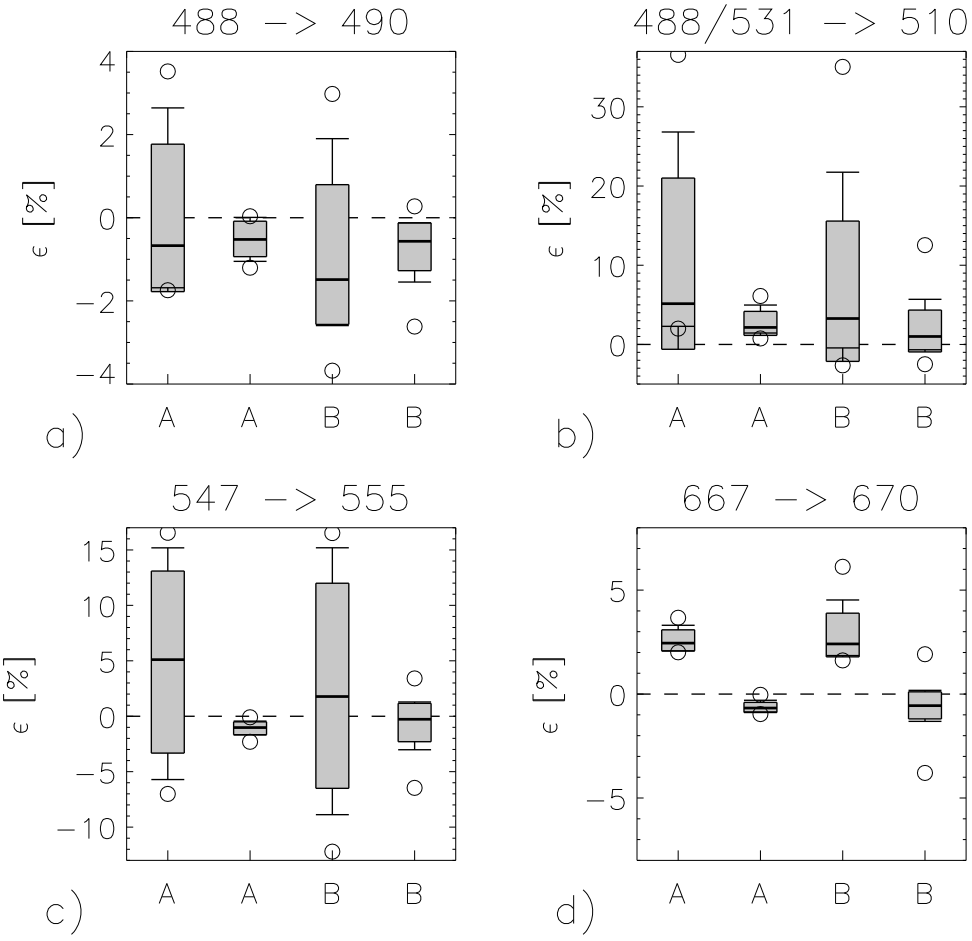

Fig. 2. Distribution of ε for selected band conversions. Statistics are displayed as box-and-whiskers plots, with boxes indicating the average $\pm$ one standard deviation, the inner bar associated with the median, and the whiskers being the 10^{th} and 90^{th} percentiles of the distributions. Minima and maxima are noted by circles. The left-hand bars are for the case of a,c,d) no correction (C_f=1), or b) linear interpolation. The right-hand bars are obtained with the band-shifting scheme. The letters A and B are associated with the Case-1 and the IOCCG synthetic data sets, respectively.

Using a simple linear interpolation to compute a R_{RS}^{int}(510) value from R_{RS} at 488 and 531 nm results in large differences, with median values of +5.1% and +3.3% for the Case-1 and IOCCG sets, respectively (Fig. 2(b)). ε is much higher for the subset Chl$a\leq$1 mg m^{-3}, with a median of +14.7% and +8.2% for the Case-1 and IOCCG sets, respectively, while the 90^{th} percentile is approximately 30%. The use of a linear interpolation results in a systematic overestimate of the

#223013 - $15.00 USD Received 11 Sep 2014; revised 7 Nov 2014; accepted 7 Nov 2014; published 28 Jan 2015

estimated R_{RS} at 510 nm for these test data sets. This is much less the case for the calculation of R_{RS}(531) by linear interpolation between 510 and 555 nm, but the inter-percentile range remains fairly high, of the order of 10%. The use of the band-shifting scheme largely reduces these differences for both conversions, the modulus of the median ε being 1% to 2% (Tables 1 and 2; 2% to 3% for Chl$a$>1 mg m^{-3}) and the inter-percentile range varying between 3% and 6%. It is interesting to assess the performance of the band-shifting scheme in fairly turbid conditions when the R_{RS} spectrum peaks at the target wavelength, which might represent a challenging condition for band shifting. Only 33 R_{RS} spectra show a maximum at 531 nm in the IOCCG data set. For these spectra, the median ε goes from -4.7% with linear interpolation to -0.6% with band shifting, in line with the overall results.

Table 2. As in Table 1 for the IOCCG data set.

$\lambda_i \rightarrow \lambda_t$	ε [%]	ε [%]; Chla$\leq$1	ε [%]; Chla>1
488 $\rightarrow$ 490	-1.5 [-2.6;+1.9]	+0.4 [-1.4;+2.4]	-2.2 [-2.9;-1.5]
(A $\rightarrow$ S/M)	-0.6 [-1.5;-0.1]	-0.2 [-0.7;-0.1]	-1.1 [-1.8;-0.4]
488/531 $\rightarrow$ 510	+3.3 [-0.4;+21.7]	+8.2 [-0.9;+28.2]	+2.4 [-0.0;+5.4]
(A $\rightarrow$ S/M)	+1.0 [-0.7;+5.7]	+0.7 [-1.0;+1.7]	+2.1 [-0.3;+7.8]
510/555 $\rightarrow$ 531	+0.3 [-4.2;+5.5]	-0.1 [-5.0;+6.4]	+0.4 [-3.6;+4.2]
(S $\rightarrow$ A)	-0.4 [-3.3;+0.7]	+0.2 [-0.9;+0.8]	-1.9 [-3.9;+0.2]
547 $\rightarrow$ 555	+1.8 [-8.9;+15.2]	+12.5 [+3.6;+15.8]	-6.5 [-9.9;-0.2]
(A $\rightarrow$ S)	-0.3 [-3.0;+1.3]	-0.1 [-0.7;+1.4]	-0.8 [-4.4;+0.9]
547 $\rightarrow$ 560	+0.9 [-14.4;+21.0]	+17.5 [+4.1;+22.8]	-11.0 [-15.9;-1.6]
(A $\rightarrow$ M)	-0.3 [-3.9;+1.9]	-0.2 [-1.1;+2.1]	-0.9 [-5.9;+1.6]
560 $\rightarrow$ 555	+0.7 [-5.5;+6.5]	-4.3 [-5.8;-0.4]	+5.0 [+1.5;+7.3]
(M $\rightarrow$ S)	+0.1 [-0.6;+1.0]	+0.1 [-0.5;+0.5]	+0.1 [-0.6;+1.8]
665 $\rightarrow$ 670	+4.8 [+3.9;+8.4]	+4.3 [+3.8;+4.8]	+6.5 [+4.7;+9.2]
(M $\rightarrow$ S)	-0.3 [-2.6;+0.6]	-0.2 [-0.6;+0.2]	-1.0 [-3.5;+0.9]
667 $\rightarrow$ 670	+2.4 [+1.9;+4.5]	+2.1 [+1.8;+2.4]	+3.4 [+2.4;+5.0]
(A $\rightarrow$ S)	-0.6 [-1.3;+0.2]	-0.6 [-0.8;-0.3]	-0.5 [-1.7;+0.5]
667 $\rightarrow$ 665	-2.3 [-3.5;-1.9]	-2.1 [-2.3;-1.9]	-2.9 [-3.8;-2.2]
(A $\rightarrow$ M)	-0.3 [-0.5;+1.4]	-0.4 [-0.5;-0.2]	+0.4 [-0.6;+2.1]

R_{RS} varies significantly in the green domain (547, 555 or 560 nm), as shown by the distribution of ε on Fig. 2(c). Differences are particularly large for Chl$a\leq$1 mg m^{-3}, with a median ε associated with the pair 547 and 555 nm of $\sim$12% for both sets (Tables 1 and 2). Operating the band-shifting scheme, the median ε is less than 1% for all conversions in the green domain, with 10^{th} and 90^{th} percentiles not exceeding 2% for the Case-1 set and 4% for the IOCCG set. The R_{RS} spectra in the IOCCG data set peak at 560 nm in 48% of the cases. In these conditions, the conversion from 547 to 560 nm is associated with a median ε that goes from -11.2% (no conversion) to -0.9%, a negligible degradation with respect to the whole data set (Table 2). With respect to ignoring the variations between bands, operating the band-shifting scheme results in an improvement in the value of $R_{RS}(\lambda_t)$ in 95% of the cases (except for the conversion 560$\rightarrow$555 for the Case-1 set, 79%).

In the red domain (665, 667 or 670 nm), the variability shown by ε is fairly limited (Fig. 2(d)). The effect of the band shifting is mainly to correct for the systematic differences resulting from the variations in the absorption coefficient by pure seawater which is a dominant factor in this spectral domain. The median ε is around 1% in modulus for all conditions after band shifting (Tables 1 and 2). Operating the band-shifting scheme results in an improvement in the value of

#223013 - $15.00 USD Received 11 Sep 2014; revised 7 Nov 2014; accepted 7 Nov 2014; published 28 Jan 2015

$R_{RS}(\lambda_t)$ in virtually all cases.

4.2. Assessment with Field Observations

The assessment of the band-shifting scheme using SeaBASS data is illustrated by Fig. 3 and Table 3. The results for a conversion between 488 and 490 nm are similar to those obtained with the synthetic data sets (compare Fig. 2(a) and 3(a)), with a reduction of the range between 10^{th} and 90^{th} percentiles for ε from 4% to 1.3% (Table 3).

When using two MODIS bands to express R_{RS} at 510 nm by linear interpolation, the values of ε are mostly positive (Fig. 3(b)) as for the synthetic data sets, with the median ε equal to +2.4% and a 90^{th} percentile value of +17%. If the band shifting is operated, the median ε is reduced to -0.2% with a 10^{th} and 90^{th} percentiles within $\pm$5%. Similar results are found when considering a shift to 531 nm using 510 and 555 nm. For the few spectra (21) that peak at 531 nm, the median ε is -0.7% after band shifting versus -4.5% if a linear interpolation is used.

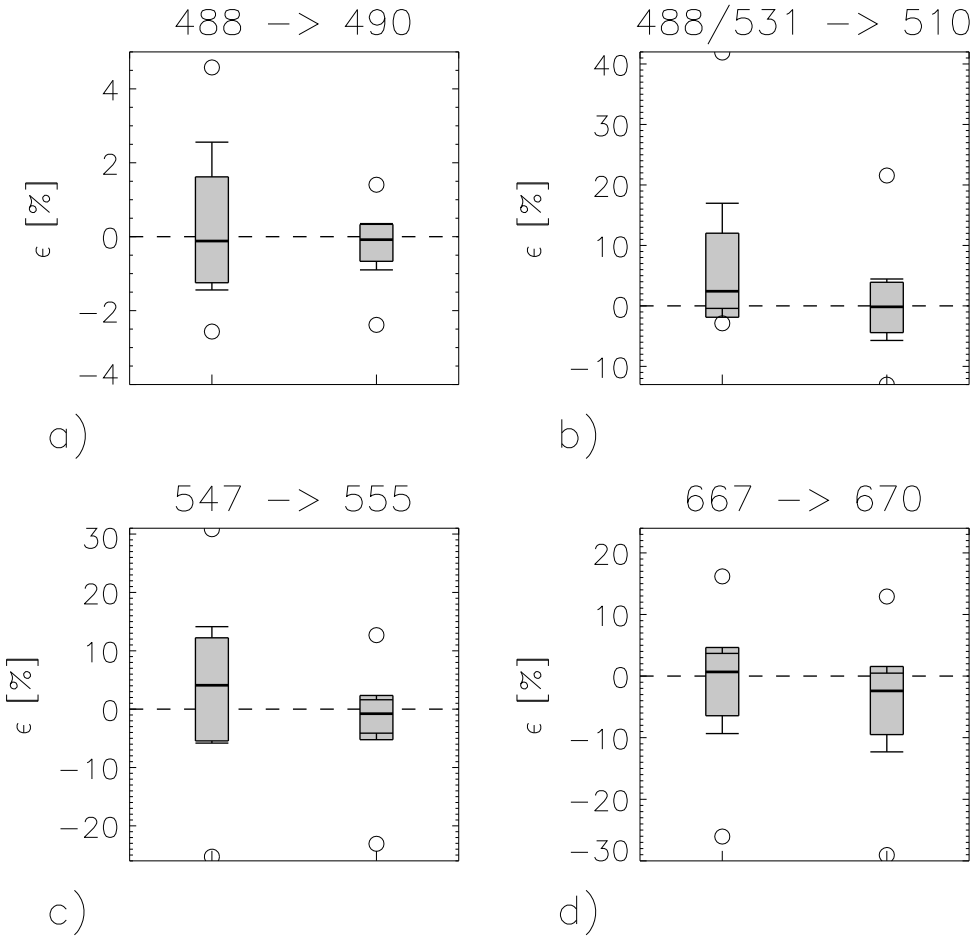

Fig. 3. Distribution of ε for selected band conversions for the SeaBASS data. Statistics are displayed as on Fig. 2.

The use of the band-shifting scheme largely reduces ε in the green domain (Fig. 3(c)). For instance, from 547 to 555 nm, the median ε is reduced from +4.1% to -0.8%. Residual variations

#223013 - $15.00 USD Received 11 Sep 2014; revised 7 Nov 2014; accepted 7 Nov 2014; published 28 Jan 2015

expressed by the 10^{th} and 90^{th} percentiles are within $\pm$5% for all conversions, much lower than in the case of no conversion (for instance, the 10^{th} and 90^{th} percentiles being -5.8% to +14.1%, respectively, for the 547 and 555-nm pair), and comparable to those observed with the IOCCG synthetic data set (Fig. 2(c)). Among the SeaBASS data, 42% of the spectra show a maximum at 560 nm; for these cases, the median ε goes from -6.1% for the case of no conversion to +0.6% after band shifting, in line with the overall results. For this spectral domain, band shifting results in an improvement in the value of the target $R_{RS}(\lambda_t)$ in 85% of the cases. In the red spectral domain, operating the band-shifting scheme on this data set does not produce any improvement. As for the synthetic data sets, the ε distribution is mostly shifted as a whole, while the inter-percentile range for the conversion 667→670 remains approximately 13% (Table 3).

Table 3. Statistics for the SeaBASS data set. For each conversion, the first line provides ε (median [10^{th};90^{th} percentiles]) for the reference case (no conversion or linear interpolation), while the second line provides the results obtained by operating the band-shifting scheme. Each conversion is indicated by the input wavelength(s) → target wavelength, together with the typical sensors for which such a conversion would be applied, with A, M and S standing for MODIS, MERIS and SeaWiFS, respectively.

$\lambda_i \rightarrow \lambda_t$	ε [%]
488 → 490	-0.1 [-1.4;+2.6]
(A → S/M)	-0.0 [-0.9;+0.4]
488/531 → 510	+2.4 [-0.4;+17.0]
(A → S/M)	-0.2 [-5.7;+4.5]
510/555 → 531	-0.3 [-3.6;+11.9]
(S → A)	+1.9 [-4.4;+4.7]
547 → 555	+4.1 [-5.8;+14.1]
(A → S)	-0.8 [-4.1;+1.6]
547 → 560	+6.0 [-9.4;+21.9]
(A → M)	-0.4 [-5.3;+3.7]
560 → 555	-1.6 [-6.4;+3.9]
(M → S)	-0.6 [-2.1;+1.2]
665 → 670	+1.7 [-13.4;+7.3]
(M → A)	-4.3 [-18.6;+1.1]
667 → 670	+0.7 [-9.3;+3.7]
(A → S)	-2.4 [-12.3;+0.5]
667 → 665	-1.0 [-3.3;+4.4]
(A → M)	+1.8 [-0.8;+7.6]

The results obtained with the MOBY data set are characterized by the small amplitude of variations in ε (Fig. 4 and Table 4). This is explained by the low variability in optical properties observed at the site, with the values of ε obtained without conversion (left-hand bars on Fig. 4) expressing the systematic differences existing between R_{RS} values at neighboring wavelengths for reflectance spectra typical of oligotrophic conditions. Operating the band-shifting scheme from 488 to 490 nm brings the ε distribution to approximately 1%. The same result is found for a conversion from 547 to 560 nm, while the median ε without conversion is +25% (Fig. 4(c)). To put these results into perspective, it can be noted that the mean relative difference between MERIS and MODIS-specific MOBY R_{RS} at 443 nm is 0.3%, which can be compared to the median ε given in Table 4 for the conversions 488→490 and 547→560, 0.7% and 1%, respectively.

#223013 - $15.00 USD Received 11 Sep 2014; revised 7 Nov 2014; accepted 7 Nov 2014; published 28 Jan 2015

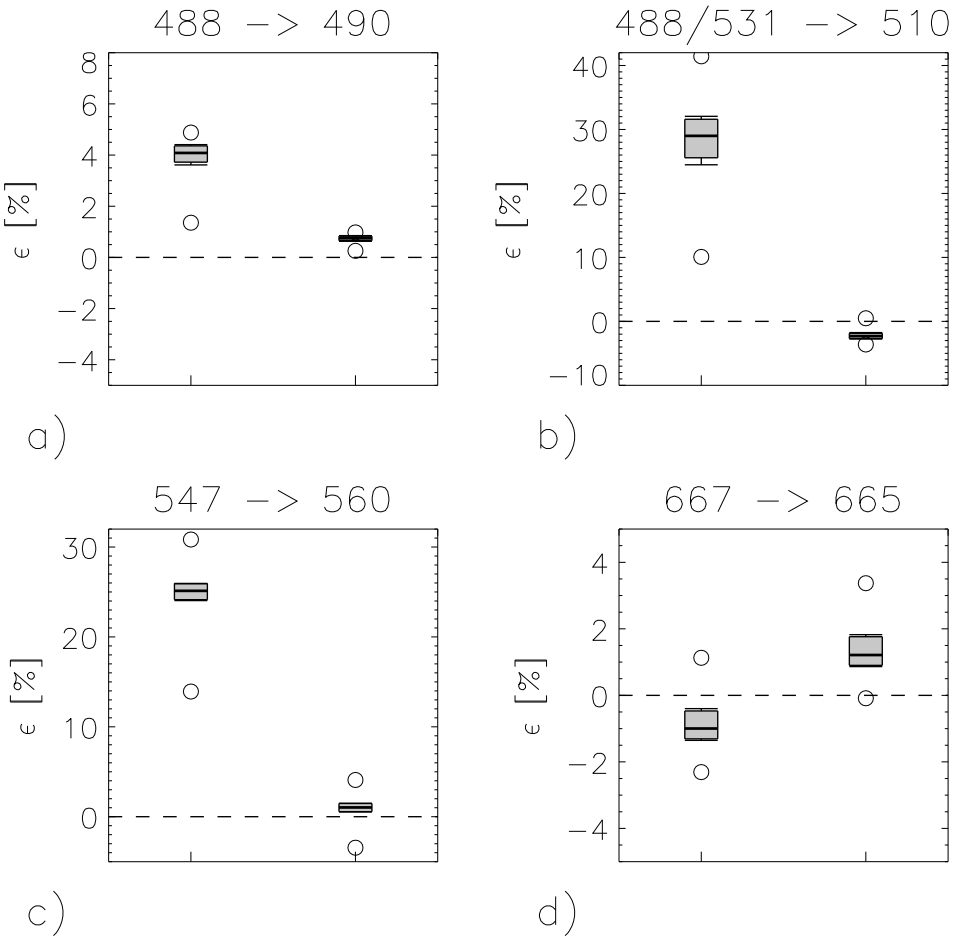

Fig. 4. Distribution of ε for selected band conversion for the MOBY data. Statistics are displayed as on Fig. 2.

Table 4. As Table 3 for the MOBY data.

$\lambda_i \rightarrow \lambda_t$	ε [%]
488 $\rightarrow$ 490	+4.1 [+3.6;+4.4]
(A $\rightarrow$ S/M)	+0.7 [+0.6;+0.9]
488/531 $\rightarrow$ 510	+29.0 [+24.5;+32.1]
(A $\rightarrow$ S/M)	-2.3 [-2.8;-1.8]
510/560 $\rightarrow$ 531	+11.8 [+10.1;+12.9]
(M $\rightarrow$ A)	+0.5 [+0.3;+0.8]
547 $\rightarrow$ 560	+25.1 [+24.0;+25.9]
(A $\rightarrow$ M)	+1.0 [+0.5;+1.5]
667 $\rightarrow$ 665	-1.0 [-1.4;-0.4]
(A $\rightarrow$ M)	+1.2 [+0.9;+1.8]

#223013 - $15.00 USD Received 11 Sep 2014; revised 7 Nov 2014; accepted 7 Nov 2014; published 28 Jan 2015

The distributions of ε are similar with and without conversion for the pair 665 and 667 nm (Fig. 4(d)), both being mostly within $\pm 1\%$. This is actually a very satisfactory result considering that the uncertainty for these bands, characterized by a low R_{RS} signal, is higher than for shorter wavelengths (exceeding 10%, [25]). The results obtained at 510 or 531 nm appear satisfactory. The application of a linear interpolation to compute a synthetic R_{RS}^{int} at 510 nm from values at 488 and 531 nm, or at 531 nm from 510 and 555 nm, produces systematic overestimates (medians of +29% and +11.8%, respectively, Table 4), whereas the band-shifting scheme shows an ε distribution within 3% and 1%, respectively. Except for the red domain, using the band-shifting scheme improves the estimate of the target R_{RS} in all cases.

4.3. Application to Satellite Data

Fig. 5 presents the average spectrum of the SeaWiFS and MODIS R_{RS} data for the coincident spectra accumulated in 2003. Band shifting has been applied to produce MODIS values associated with the SeaWiFS bands for the 4 upper wavelengths, 490, 510, 555 and 670 nm. Their average values show a close agreement with the SeaWiFS values. At 490, 555 and 670 nm, the average converted MODIS value has been shifted closer to the SeaWiFS value, while the average MODIS R_{RS} at 510 nm is also comparable to its SeaWiFS counterpart. It is worth noting that a direct linear interpolation between 488 and 531 nm would produce a R_{RS} at 510 nm significantly higher that the result obtained through the band-shifting scheme, which is consistent with the overestimates shown by the reflectance obtained by linear interpolation R_{RS}^{int} in the assessments with synthetic or field data.

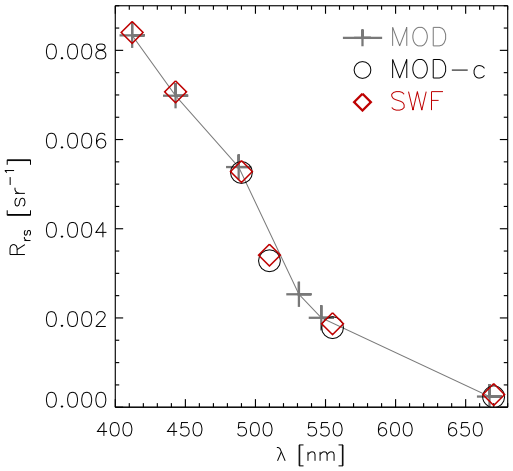

Fig. 5. Average of all coincident spectra for the SeaWiFS data (red diamonds), the original MODIS data (grey line and crosses) and MODIS band-shifted data (black circles).

More detailed comparison statistics are shown by frequency distributions of the ratio between MODIS and SeaWiFS R_{RS} (Fig. 6). At 412 and 443 nm where no band shifting is operated, the median ratio μ is very close to 1 (1.002 and 0.997, respectively). Band shifting slightly improves the agreement between the two products at 490 nm: while the median ratio between the MODIS $R_{RS}(488)$ and the SeaWiFS $R_{RS}(490)$ is 1.030, it is reduced to 1.007 when the MODIS R_{RS} is expressed at 490 nm (Fig. 6(c)). For the green bands, separated by 8 nm, the changes are larger, with μ decreasing from 1.108 to 0.978 (Fig. 6(e)). On the other hand, no

#223013 - $15.00 USD Received 11 Sep 2014; revised 7 Nov 2014; accepted 7 Nov 2014; published 28 Jan 2015

changes are noticeable in the red part of the spectrum (μ approximately equal to 0.9). For this band, R_{RS} values are low for a large part of the ocean, and relative differences are likely to become larger than for other bands, which is translated here by a broad distribution of the frequency distribution. Frequency distributions of the ratio between the MODIS R_{RS} at 488 or 531 nm and the SeaWiFS R_{RS} at 510 nm are expectedly far from 1 (μ equal to 1.607 and 0.728, respectively). The operation of the band shifting produces a MODIS R_{RS} at 510 nm fairly close to the SeaWiFS distribution: not only is the median ratio close to 1 (μ equal to 0.979) but the width of the frequency distribution is comparable to other bands (Fig. 6(d); the standard deviation is 0.25 versus 0.24 at 443 nm). Results obtained with the satellite data are thus encouraging. It should also be noted that in this exercise the errors associated with the band-shifting scheme cannot be separated from actual differences between sensor-specific products.

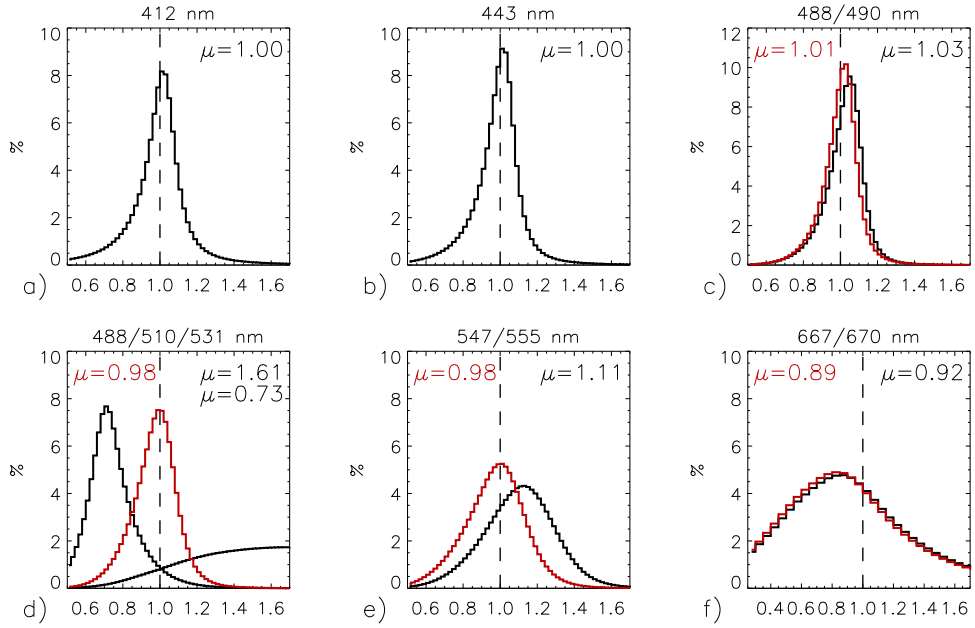

Fig. 6. Frequency distribution of the ratio between MODIS and SeaWiFS R_{RS}. Black curves and statistics (median ratio μ) are for comparisons with the original data, while red curves and statistics are based on MODIS values expressed onto the SeaWiFS bands by the band-shifting scheme.

5. Conclusions

An approach has been proposed to handle differences in nominal center-wavelengths between reflectance spectra. It is intended for remote sensing applications or validation studies with broadly distributed data. The evaluation presented here is the first of its kind and can serve as a benchmark when other approaches will be proposed. The scheme has been tested on synthetic data as well as field observations, which altogether cover a large domain of optical conditions. The relative error ε on the conversion factors from 488 to 490 nm is mostly within $\pm$1%. The range of ε is within $\pm$2% for conversions between green bands for the MOBY data set and for the synthetic data, even though it tends to increase for high Chl*a* values (see Table 2). For the SeaBASS data set, ε values for the green bands are generally within $\pm$5%, which is comparable

#223013 - $15.00 USD Received 11 Sep 2014; revised 7 Nov 2014; accepted 7 Nov 2014; published 28 Jan 2015

to accuracy objectives for satellite R_{RS} [31], while the median ε is less than 1% (in modulus) like for the other data sets. Results obtained at 510 nm are as well satisfactory, with differences with respect to target values generally lower than $\pm$5%. This level of agreement is reached by operating the band shifting from 488 to 510 nm, and from 531 to 510 nm, and then calculating a weighted average of the two values (Eq. (8)). The combination of these two band-shifting operations is justified by the fact that the spectral distance is similar on both sides of 510 nm ($\sim$20 nm) and allows some compensation of errors as the band shifting operates towards longer and shorter wavelengths. Slightly better results are obtained when R_{RS} is computed at 531 nm from values at 510 and 555 nm. The distribution of ε associated with conversions in the red part of the spectral domain is usually within 1% for the synthetic data, whereas no improvement can be noticed when field observations or satellite data are used. This might be partly explained by higher uncertainties in that wavelength range. In the case of the assessment with simulated data, it is worth noting that all band-shifting operations are characterized by an inter-percentile range within 2% for all conversions for Chl*a* lower than 1 mg m^{-3}, which is the condition encountered in most of the global ocean (Tables 1 and 2). These results are obtained with QAA version 5 but are not significantly affected with version 6.

The band-shifting scheme has been applied to a year-worth of global MODIS and SeaWiFS data with encouraging results. The differences between R_{RS} from the two missions are reduced at 490 and 555 nm, and the agreement found at 510 nm, together with the results observed with the synthetic or in-situ data sets, supports the possibility of producing synthetic MODIS reflectance at that band. Based on these results, the ocean color component of the European Space Agency Climate Change Initiative [32] has adopted this scheme to produce a multi-mission data records of marine reflectance (MERIS, MODIS-Aqua and SeaWiFS) at a common set of bands. In that context, band shifting allows a comprehensive comparison of R_{RS} products and their merging into a consistent data record.

The approach proposed here to operate band shifting relies on the inversion of a bio-optical model to compute a set of IOPs, and its subsequent use in forward mode to determine a reflectance value at a target wavelength. Other algorithms could be used in that framework, for instance those relying on a non-linear inversion (e.g., [33, 34]) to simultaneously retrieve a set of optical properties or concentrations of optically significant constituents. These are usually made of three variables, associated with absorption by phytoplankton and CDM, and particle backscattering, that constitute the degrees of freedom of the model. After inversion, the model can be operated in forward mode to calculate R_{RS} at any wavelength, a two-step process that has been explored in the context of data merging [35, 36]. In that case, it is worth bearing in mind that output R_{RS} values are constrained to a family of spectral shapes defined by the degrees of freedom and the specific inherent optical properties of the bio-optical model, so that R_{RS} computed at the original wavelengths are no longer equal to the input R_{RS}.

Purely mathematical methods could be envisaged for the purpose of band shifting. Tentative tests with a cubic spline interpolation has led to mixed results. When applied to the SeaBASS data set, results are similar for blue and green bands to those of Table 3 (with a median ε not differing by more than 0.5%), with the exception of the shifting at 510 nm with the median $|\varepsilon|$ larger by 3%. On the other hand, median ε values are higher by 6% to 20% for conversions in the red part of the spectrum. When compared to Table 4 associated with the MOBY data, the median ε is higher by approximately 20% for conversions to 510 or 531 nm, is equal to -6.1% for the conversion from 547 to 560 nm, and exceeds -100% for the conversion from 667 to 665 nm. While it is recognized that advanced mathematical techniques could provide improved results, the current optically-based approach appears more suitable to handle a wide set of cases.

In any case, albeit the selected model (QAA) performs well with respect to other algorithms

#223013 - $15.00 USD Received 11 Sep 2014; revised 7 Nov 2014; accepted 7 Nov 2014; published 28 Jan 2015

[22, 19, 20], optical model developments could further enhance the performance of the band shifting by improving the retrieval of IOPs and the representation of their spectral shape. The latter could be allowed to vary regionally so as to capture spatial variations in specific optical properties [6]. Improvements should be sought for eutrophic and coastal waters as the results of the band-shifting assessment showed degraded statistics in some cases for high Chl*a* values (Tables 1 and 2). Cases of extremely turbid waters should also be tested.

Besides presenting a band-shifting scheme, this work highlights how differences in center wavelengths of the order of a few nanometers are associated with significant differences in reflectance, even though R_{RS} values at neighboring bands have been shown to be highly correlated [37]. Between 488 and 490 nm, differences of 1% to 2% are typical, increasing to 3-4% in oligotrophic conditions (Tables 1 and 4). In the green spectral region, differences can be much higher, typically above 5% but potentially exceeding 15% in oligotrophic conditions. Accounting for band differences is thus a prerequisite for a thorough assessment of the multi-mission ocean color data record as well as time series analysis [38], and band shifting is becoming a standard practice in validation studies. Ultimately, considering the stringent requirements of climate research, efforts should be dedicated to fully include in the treatment of ocean color data the subtle impacts that the spectral response of each sensor can exert on the reflectance spectra [39, 40]. Finally, more high-quality hyper-spectral field observations should be collected in diversified environments, particularly those associated with optical extremes; besides their applications in terms of bio-optical modeling, they are essential to testing band-shifting approaches.

Acknowledgments

This work is contributing to the Ocean Colour Climate Change Initiative (OC-CCI) of the European Space Agency. NASA is thanked for SeaBASS and the availability of ocean color satellite data. The contribution to SeaBASS of individual PIs is acknowledged, N. Nelson and D. Siegel (for BBOP data), D. Pirhalla, R. Stumpf, P. Tester (for NOAA data), R. Arnone, W. Goode, R. Gould, R. Green, D. Johnson, S. Ladner, Z.-P. Lee, B. Lubac, W. Rhea, A. Weideman (for NRL data), G. Arias, L. Guzman, C. Hu, L. Lorenzoni, M. McIntyre, F. Muller-Karger, A. Odriozola, R. Varela (for USF data). The MOBy programme, currently supported by NOAA, and K. Voss and K. Hughes are earnestly thanked for the availability of the data.

#223013 - $15.00 USD Received 11 Sep 2014; revised 7 Nov 2014; accepted 7 Nov 2014; published 28 Jan 2015